Tool Geometry for Friction Stir Welding—Optimum Shoulder Diameter

M. MEHTA, A. ARORA, A. DE, and T. DEBROY

The most important geometric parameter in the friction stir welding (FSW) tool design is the shoulder diameter, which is currently estimated by trial and error. Here, we report a combined experimental and theoretical investigation on the influence of shoulder diameter on thermal cycles, peak temperatures, power requirements, and torque during FSW of AA7075-T6. An optimum tool shoulder diameter is identified using a three-dimensional, heat transfer and materials flow model. First, the predictive capability of the model is tested by comparing the computed values of peak temperature, spindle power, and torque requirements for various shoulder diameters against the corresponding experimental data. The change in the values of these variables with shoulder diameter is correctly predicted by the model. The model is then used to identify the optimum tool shoulder diameter that facilitates maximal use of the supplied torque in overcoming interfacial sticking. The tool with optimum shoulder diameter is shown to result in acceptable yield strength (YS) and ductility.

I. INTRODUCTION

ALTHOUGH friction stir welding (FSW) is now widely used for the joining of aluminum and other soft alloys, its commercial application to hard materials such as steels and titanium alloys is still developing.[1–5] An important challenge is to develop cost-effective tools with reliable and long service life.[1,6] No unified approach for tool design based on the scientific principles is now available in the literature.[1] The current practice for tool selection involves the intuitive choice of tool material with higher softening temperature and tensile strength than those of the workpiece material.

Most of the previous research on the geometry of the tool has focused on the tool pin. Buffa et al.[7] showed by finite element calculations that an increase in pin taper angle resulted in higher peak temperature. Fujii et al.[8] showed that a columnar tool pin without any thread resulted in defect-free welds in soft alloys such as AA1050, while a triangular prism-shaped tool pin was appropriate for hard alloys such as AA5083. Kumar and Kailas[9] suggested that the material flow induced by the pin is important to achieve a cavity-free weld joint. Zhao et al.[10,11] showed that a threaded tapered pin profile produced welds with minimum defects in AA2014. Hattingh et al.[12] suggested a relation between the thread pitch, pin diameter, and plate thickness to achieve sound welds for trifluted tapered pins. Thomas

et al.[13,14] suggested that the tapered threads in WHORL* pin design induce a vertical material flow.

*WHORL is a trademark of The Welding Institute, Abington, Cambridge.

Furthermore, the larger surface of the MX TRIFLUTE** tool leads to higher heat generation

**MX TRIFLUTE is a trademark of The Welding Institute, Abington, Cambridge.

rates and improved material flow.[13,14] Colegrove and Shercliff[15,16] suggested that the TRIFLUTE pin increased the downward material flow based on modeling. Although the role of pin geometry has been addressed in several studies, the effect of the tool shoulder geometry during FSW is not well understood.

Among the various geometric features of an FSW tool, the size of the shoulder is by far the most important.[1,6] The shoulder generates most of the heat, induces flow of plasticized materials, and prevents its escape from the workpiece during welding.[3–5] The stronger the workpiece material, the greater is the need for the shoulder to generate heat for adequate softening and ease of material flow around the tool pin.[1,6–17] Larger shoulder diameter also requires higher spindle power and torque. In order to achieve a long tool life, the tool shoulder should facilitate adequate softening and ease of flow of workpiece materials while requiring low power and torque. A unified method to determine the optimum shoulder diameter considering such contrasting requirements has not been reported so far in the literature.

Zhang et al.[18] suggested that larger shoulder diameters would result in higher peak temperatures based on

M. MEHTA, PhD Student, and A. DE, Professor, are with the Department of Mechanical Engineering, Indian Institute of Technology, Bombay, Mumbai 400076, India. A. ARORA, PhD Candidate, and T. DEBROY, Professor, are with the Department of Materials Science and Engineering, The Pennsylvania State University, University Park, PA 16802. Contact e-mail: debroy@psu.edu

finite element calculations using commercial software. The shoulder roughness is also thought to be important in preventing the escape of flush from the weld.[19,20] Elangovan and Balasubramanian[21] studied the effect of tool shoulder diameter on the mechanical properties and found that one of the three diameters resulted in superior weld tensile properties during FSW of AA6061. Although the reason for this behavior is not well understood, we found that welds with best properties corresponded to maximum utilization of the supplied torque in overcoming sticking.[22] In short, the previous research has established the importance of shoulder geometry in both the operation of the FSW process and the resulting properties of the welded joints.

Here, we show experimentally and theoretically that a criterion that balances the need for low flow stress for good material flow and the contrasting requirement for the tool to have a good grip on the plasticized material can be used to identify an optimum shoulder diameter. In order to verify this approach, we performed FSW experiments on AA7075-T6 for a number of tool shoulder diameters and tool rotational speeds and used a three-dimensional, heat transfer and viscoplastic flow model to simulate these welding experiments. The computed results are extensively validated with the corresponding experimentally measured values of peak temperature, thermal cycles, and torque and power requirements for several combinations of shoulder diameter and tool rotational speeds. After validation of the model, it was used to calculate the optimum shoulder diameters for each rotational speed. We further show that the use of tools with optimum shoulder diameter results in acceptable yield strength (YS) and ductility of the welded joints. In addition, the optimum shoulder diameter tools are also shown to have adequate torsional strength to endure large torques without any distortion or failure.

II. EXPERIMENTAL DETAILS

Aluminum alloy AA7075-T6 plates 172-mm long, 97-mm wide, and 3.5-mm thick are welded in a square butt joint configuration. A 25-mm-thick AISI316 back-up plate is used, which reduces the heat loss from the bottom face because of the low thermal conductivity (around 16 W/mK at 373 K [100 °C] and 21 W/mK at 773 K [500 °C]) of stainless steel. Table I shows the compositions of the workpiece and tool materials. Five tools with different shoulder diameters with the same cylindrically tapered pin geometry were used for the welds. Table II presents the tool shoulder and the pin dimensions. All welds were made with a tool tilt angle of 2 deg. Transient temperature during welding was measured at three monitoring locations: two on the advancing side and one on the retreating side, positioned at a transverse distance of 8.5 mm from the butting surface and depth of 0.75 mm from the top surface. The two K-type thermocouples in the advancing side were kept 50 mm apart in the direction of welding to examine the accuracy of the measured temperature profiles. The tool spindle power was measured using two watt-meters. The torque used by the tool was obtained by dividing the spindle power with the corresponding tool rotational speed (rad/s). The ultimate tensile strength (UTS), YS, and percent elongation (at break) were determined from the transverse section of the welded specimens.

III. THEORETICAL FORMULATION

A three-dimensional, heat-transfer and viscoplastic flow model for FSW is used for the calculations. The details of the model and the computed results for the welding of various alloys were reported earlier.[3–5,23–26] A few salient features of the model are explained here. The model solves the equations of conservation of mass, momentum, and energy in steady-state, three-dimensional Cartesian coordinate considering incompressible single phase flow.[23–26] The following energy conservation equation is solved.[23–26]

$$\rho C_p \frac{\partial(u_i T)}{\partial x_i} = -\rho C_p U_1 \frac{\partial T}{\partial x_1} + \frac{\partial}{\partial x_i}\left(k\frac{\partial T}{\partial x_i}\right) + S_{in} + S_b \quad [1]$$

Table II. Tool Dimensions, Welding Parameters, and Workpiece Material Properties Used for Calculations

Workpiece material	AA 7075
Tool material	EN24 tool steel
Tool shoulder diameter (mm)	15, 20, 25, 30, 35
Pin diameter at root (mm)	6.0
Pin diameter at tip (mm)	4.66
Pin length (mm)	3.325
Workpiece thickness (mm)	3.5
Tool rotational speed (rpm)	355, 450, 560, 710
Welding speed (mm s^{-1})	0.67
Axial pressure (MPa)	30.0
Workpiece solidus temperature (K (°C))	749 (476)
Specific heat* (J kg^{-1} K^{-1})	$0.20 - 3.0 \times 10^{-4}T + 1.0 \times 10^{-7}T^2 - 3.0 \times 10^{-12}T^3$
Thermal conductivity* (W m^{-1} K^{-1})	$0.18 + 6.0 \times 10^{-4}T - 1.0 \times 10^{-7}T^2$
Yield stress (MPa)	$6.97 \times 10^3 \times e^{(-0.0087 \times T)}$ for $T < 644$ K $0.285 \times (749 - T)$ for $644 < T < 749$ K

Table I. Composition of Workpiece (AA 7075) and Tool (EN24) Materials

AA7075	element	Al	Cu	Mg	Zn	Cr
	wt pct	90	1.6	2.5	5.6	0.23
EN24	element	C	Mn	Ni	Cr	Mo
	wt pct	0.35 to 0.45	0.45 to 0.70	1.30 to 1.80	0.90 to 1.40	0.20 to 0.35

where ρ is the density of the material; C_P and k are the temperature-dependent specific heat and thermal conductivity of the material, respectively; u_i is the velocity component; T is the temperature; U_1 is the welding velocity; and S_{in} and S_b are the source terms due to interfacial heat generation per unit volume at the tool-workpiece interface and heat generation rate due to plastic deformation in the workpiece away from the interface, respectively. The rate of heat generation at the tool-workpiece interface is obtained from the following relation:[23–26]

$$S_{in} = \left[(1 - \delta)\eta\tau + \delta\mu_f P_N\right](\omega r - U_1 \sin\theta) \qquad [2]$$

where δ and μ_f are spatially variable fractional slip and coefficient of friction between the tool and the workpiece, respectively; η is the mechanical efficiency; τ is the shear stress at yielding; P_N is the axial pressure; ω is the tool rotation speed; r is the radial distance from the tool axis; and θ is the angle with the direction of movement of the tool. The term $(\omega r - U_1 \sin\theta)$ represents the local velocity of a point on tool with the origin fixed at the tool axis. The spatial variations of fractional slip, δ, and the coefficient of friction, μ_f, in Eq. [2] are derived from the trend of the reported data on accumulated slip during cross-wedge rolling as[27]

$$\delta = 0.31 \times \exp\left(\frac{\omega r}{1.87}\right) - 0.026 \qquad [3]$$

$$\mu_f = 0.5 \times \exp(-\delta\omega r) \qquad [4]$$

where ωr is in meters per second. Equations [3] and [4] are valid for ωr from 0.1 to 1.6 m/s, as reported in the literature.[27] The local heat generation due to plastic deformation, S_b, is computed as $\lambda\mu\dot{\varepsilon}^2$, where μ is the viscosity, $\dot{\varepsilon}$ is the effective strain rate, and λ is a constant that indicates the fraction of plastic work that is converted to heat. The spatially variable strain rate $\dot{\varepsilon}$ is computed as follows:

$$\dot{\varepsilon} = \sqrt{\frac{2}{3}\left(\left(\frac{\partial u_i}{\partial x_i}\right)^2 + \frac{1}{2}\left(\frac{\partial u_1}{\partial x_2} + \frac{\partial u_2}{\partial x_1}\right)^2 + \frac{1}{2}\left(\frac{\partial u_1}{\partial x_3} + \frac{\partial u_3}{\partial x_1}\right)^2 + \frac{1}{2}\left(\frac{\partial u_3}{\partial x_2} + \frac{\partial u_2}{\partial x_3}\right)^2\right)} \qquad [5]$$

where u_i is the velocity component with $i = 1, 2$, and 3 referring to the three axes in the Cartesian coordinate system. The torque (M) required during FSW is computed as

$$M = M_T + M_L \qquad [6]$$

where M_T and M_L are the fractions of the total torque responsible for material flow by overcoming sticking and frictional heating by sliding, respectively. Hereafter, M_T and M_L are referred to as sticking torque and sliding torque, respectively, and are computed as follows:

$$M_T = \oint_A r_A \times (1 - \delta)\tau \times dA \qquad [7]$$

$$M_L = \oint_A r_A \times \delta\mu_f P_N \times dA \qquad [8]$$

where r_A is the distance of any infinitesimal area element, dA, from the tool axis. As indicated in Eq. [2], both components of the torque contribute to heat generation. The spindle power is calculated as follows:

$$P = \oint_A \left\{(1 - \delta)\tau + \delta\mu_f P_N\right\}\omega r_A dA \qquad [9]$$

IV. RESULTS AND DISCUSSION

Figure 1 shows a comparison between the computed and the corresponding measured values of peak temperatures at various shoulder diameters for rotational speeds 355 and 560 rpm. The tool dimensions, welding conditions, and material properties used for the calculation are presented in Table II. It is observed that the peak temperature increases with the increase in shoulder diameter and tool rotational speed. A larger shoulder diameter provides greater contact area, resulting in higher frictional and mechanical work that leads to higher temperature. Both the computed and the experimental results also show that the effect of shoulder diameter is more pronounced than that of the rotational speed. Figure 2 shows a comparison between the experimentally measured and the corresponding computed thermal cycles for a tool shoulder diameter of 20 mm and a rotational speed of 355 rpm. A fair agreement between the computed and corresponding measured peak temperature and thermal cycles indicates that the model is capable of predicting these variables correctly.

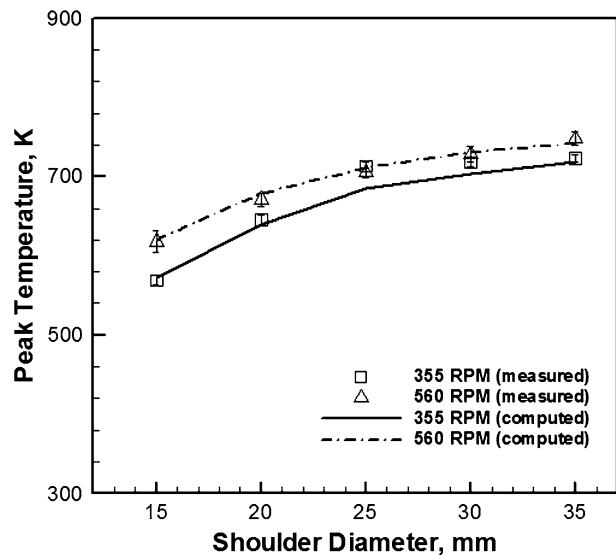Figure 3 shows the computed and the corresponding measured torque required during FSW. The torque

Fig. 1—Comparison of the measured and computed peak temperatures during FSW of AA7075-T6 at rotational speeds of 355 and 560 rpm. The error bars shown represent the error in measurement estimated by repeated measurements.
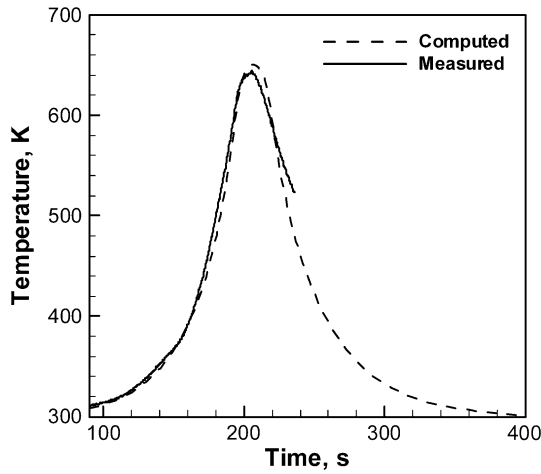
Fig. 2—Comparison of the computed and the measured time-temperature profiles at a location 8.5 mm away from the butting surface and 0.75 mm from the top surface in the advancing side for the friction stir welding of AA7075-T6 with a 20-mm shoulder diameter tool at 355 rpm.
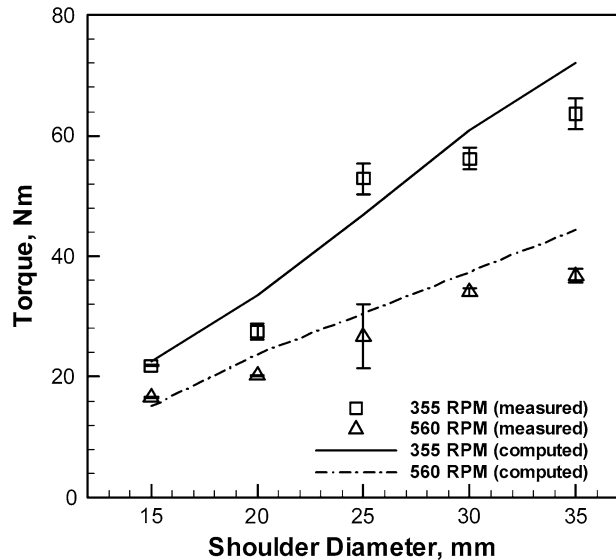

Fig. 3—Comparison of the measured and computed torque required for FSW of AA7075-T6 at rotational speeds of 355 and 560 rpm. The error bars shown represent the error in measurement estimated by repeated measurements.

increases with the increase in the shoulder diameter and decrease in the rotational speed. The effect of rotational speed is more prominent at larger shoulder diameters. Increase in the tool-workpiece contact area with the shoulder diameter leads to higher torque requirement, as shown in Eqs. [7] and [8]. Fractional slip increases significantly with rotational speed and shoulder radius, as shown in Eq. [3]. However, the friction coefficient decreases exponentially as fractional slip, rotational speed, or shoulder radius increase, as shown in Eq. [4]. With the increase in rotational speed, the fractional slip increases, and as a result, the sticking torque decreases significantly. The increased rotational speed and fractional slip also lead to lower friction coefficient and
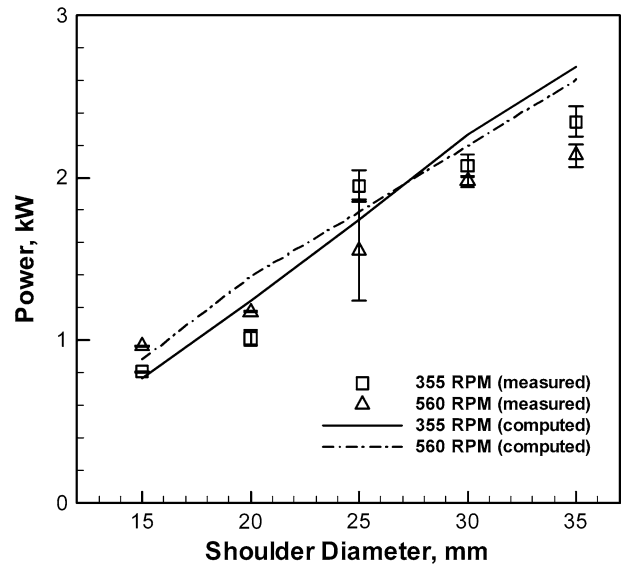

Fig. 4—Comparison of the measured and computed power required for FSW of AA7075-T6 at rotational speeds of 355 and 560 rpm. The error bars shown represent the error in measurement estimated by repeated measurements.

reduction in sliding torque. Figure 4 shows the computed and the corresponding measured values of spindle power as a function of shoulder diameter. The power requirement increases with shoulder diameter due to the increase in the tool workpiece contact area. In contrast, there is no significant effect of rotational speed on the spindle power. Figures 3 and 4 show a fair agreement between the measured and the corresponding computed values of torque and power required for welding.

The tool life is affected by the flow stress and temperature of the deforming material near the tool.[28,29] The volume averaged characteristic flow stress, σ_z, and temperature, T_z, of the deforming material can be calculated as

$$\sigma_z = \frac{\sum \sigma \times V}{\sum V} \qquad [10]$$

$$T_z = \frac{\sum T \times V}{\sum V} \qquad [11]$$

where σ and T are the flow stress and temperature of a location in the deforming zone, respectively, and V is the corresponding cell volume. Figure 5 shows the characteristic flow stress and temperature combinations experienced by the deforming material at various shoulder diameters and rotational speeds. It is observed that the characteristic temperature increases with increase in shoulder diameter. This trend is similar to the observed trend in the peak temperature with shoulder diameter shown in Figure 1. Consequently, the characteristic flow stress reduces with increase in shoulder diameter. Figure 5 suggests lower resistance to a larger shoulder diameter tool during deformation of the workpiece material. However, the torque required is comparatively higher for larger shoulder diameter tools, as shown in Figure 3. Thus, when the shoulder diameter is increased,
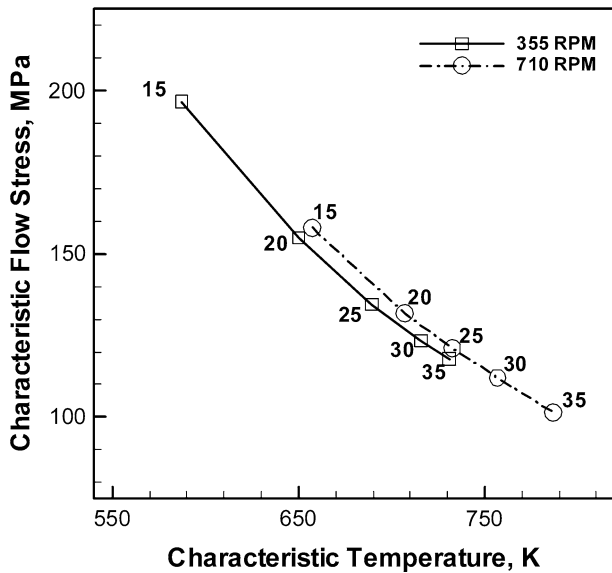
Fig. 5—Characteristic flow stress and temperature of the deforming material near the tool for various shoulder diameters and rotational speeds. The legends near the symbols are shoulder diameters in millimeters.

Fig. 6—Computed values of sticking torque *vs* shoulder diameter for various tool rotational speeds. All other welding parameters, presented in Table II, remain constant.

the lower resistance to deformation is achieved at the expense of higher total torque requirement.

The torque provided by the tool is used for sliding and to overcome sticking during welding. The sliding torque continuously increases with shoulder diameter due to larger contact area, as indicated in Eq. [8]. The sticking torque is affected by both contact area and shear strength, τ, as shown in Eq. [7]. With an increase in the shoulder diameter, the contact area increases while the shear strength reduces. Thus, with an increase in shoulder diameter, the sticking torque first increases, reaches a maxima, and then decreases because the shear strength decreases with increase in temperature. Figure 6 shows the sticking torque *vs* shoulder diameter for various tool rotational speeds. The shoulder diameter corresponding to the maximum sticking torque is taken as the optimum shoulder diameter for each rpm. All other welding variables were kept constant. Figure 6 shows that the optimum values of the shoulder diameter are 30, 25, and 20 mm corresponding to the rotational speeds 355, 560, and 710 rpm, respectively. Since the torque components are dependent on various parameters apart from the tool rotational speed, these estimated optimum shoulder diameter values are valid for the process parameters considered here. The values of peak temperature corresponding to these optimum conditions are 713 K, 705 K, and 719 K (440 °C, 432 °C, and 446 °C), respectively. All these peak temperatures lie in the range of 0.94 to 0.96 T_S, where T_S is the solidus temperature (749 K [476 °C]). This range lies well within the suggested working temperatures for FSW.[1,6,13,28,29]

During the torque calculations, we observed that the two torque components are equal when the sticking torque is maximum. Although the reason for this equality is not known, the following discussion will show that an objective function based on the two torque
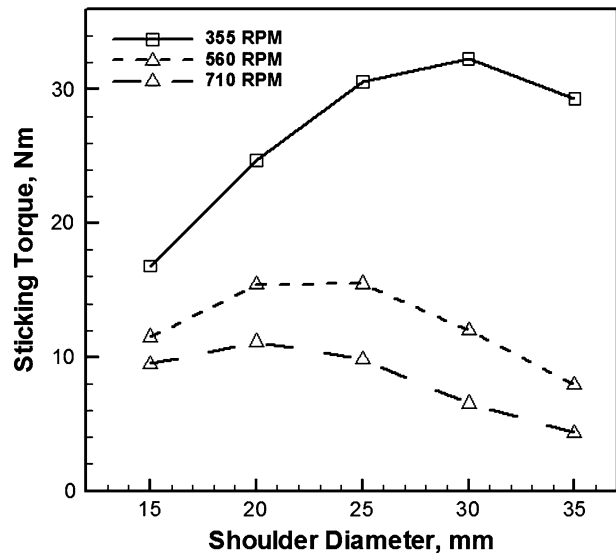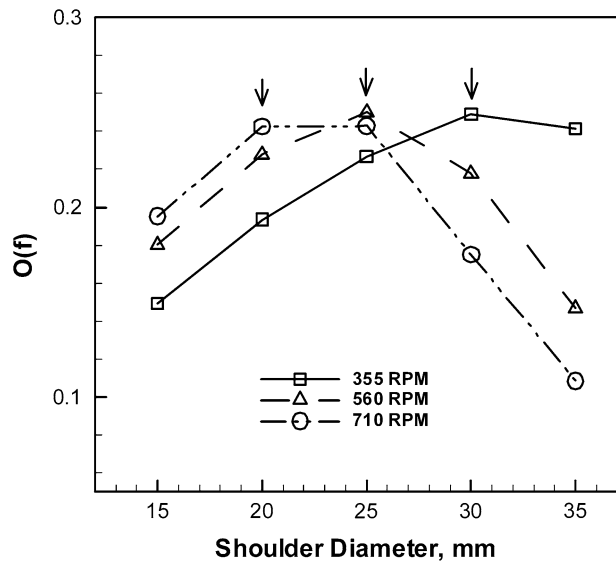

Fig. 7—Variation of the objective function, $O(f)$, as a function of tool shoulder diameter at various tool rotational speeds.

components gives the same optimum shoulder diameter as given by the maximum sticking torque. The objective function, $O(f)$, can be defined as shown subsequently:

$$O(f) = \left(\frac{M_T}{M_T + M_L} \times \frac{M_L}{M_T + M_L} \right) \qquad [12]$$

where M_T and M_L are the sticking and sliding torques defined by Eqs. [7] and [9], respectively. The two terms on the right-hand side of Eq. [12] represent the sticking and sliding fractions of the total torque. Figure 7 shows the computed values of $O(f)$ as a function of the tool shoulder diameter for three rotational speeds.
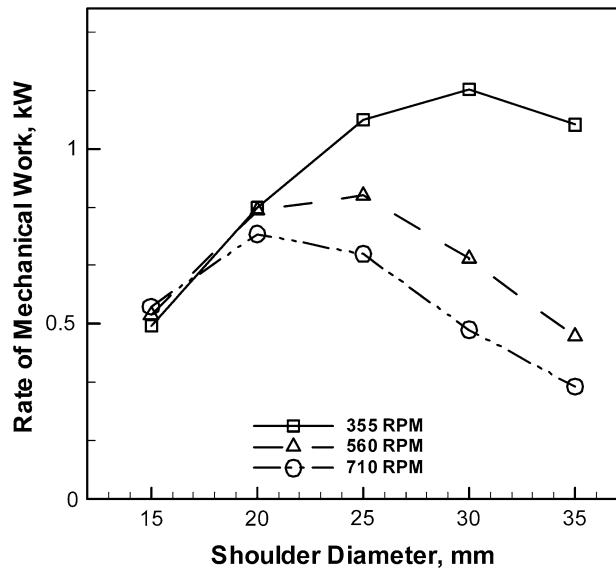
Fig. 8—Computed values of rate of mechanical work done at varying shoulder diameters for rotational speeds of 355, 560, and 710 rpm.
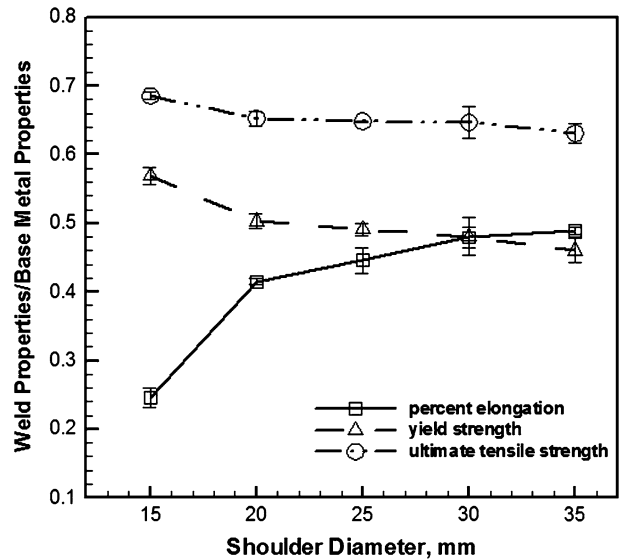

Fig. 9—Ratio of the weld joint percent elongation, YS, and UTS to the corresponding base metal properties. The weld was made using tool rotational speed 355 and 0.67 mm/s.

The function $O(f)$ has a maximum value of 0.25 when the sticking and sliding torques are equal. The figure shows that the $O(f)$ is maximum at the shoulder diameter of 30, 25, and 20 mm corresponding to the rotational speeds 355, 560, and 710 rpm, respectively. These values of shoulder diameter for the given rotational speeds are the same as the optimum shoulder diameter obtained from maximizing the sticking torque. The value of the optimum shoulder diameter decreases with the increase in the tool rotational speed. For higher tool rotational speeds, a smaller tool shoulder diameter is sufficient to provide enough heat to soften the material and induce the flow. However, a larger tool shoulder is required for the same purpose at lower rotational speeds. As the tool shoulder diameter increases beyond the optimum shoulder diameter, the relative velocity of the tool and workpiece increases, leading to higher slip. This increased value of slip leads to lower sticking torque and reduced grip of the tool on the workpiece.

The role of shoulder diameter can be further studied by evaluating the computed rate of mechanical work, which is calculated by the first term $[(1 - \delta)\eta\tau(\omega r - U_1 \sin\theta)]$ in Eq. [2]. Figure 8 shows that the maximum rate of mechanical work is done when the shoulder diameter is optimum. Beyond the optimum shoulder diameter, the rate of mechanical work decreases. However, the total power increases continuously with shoulder diameter, as shown in Figure 4, due to the increase in the rate of sliding frictional work.

Loss of the YS and the ductility of the welded joints in comparison with the corresponding properties of the base material are important for aluminum alloys. For example, Mahoney et al.[30] reported a moderate to significant loss in the UTS and YS in FSW of AA7075-T651. Figure 9 shows the influence of shoulder diameter on the YS and UTS of the welds and the percent elongation (at break), welded at a tool rotational speed of 355 rpm and a welding velocity of 0.67 mm/s.

The ratio of the weld joint property to the corresponding base material property is shown in the figure for various tool shoulder diameters. The percent elongation at break, YS, and UTS for the AA7075-T6 base material are 11 to 12 pct, 503 MPa, and 572 MPa, respectively. As shown in Figure 9, the YS of the weld joint is 57 pct of the base material YS when the 15-mm shoulder diameter tool is used and is about 46 pct of the base material YS when the 35-mm shoulder diameter tool is used. The percent elongation changes from 25 to 49 pct of the base material as the shoulder diameter increases from 15 to 35 mm. The YS and percent elongation of the weld joint is 48 pct of the base material properties when the tool with optimum shoulder diameter of 30 mm is used. These weld properties obtained from use of tool with optimum shoulder diameter are within the range of commonly obtained weld properties.[30]

Considering the FSW tool as a solid circular shaft, the computed total torque for the optimum shoulder diameter can be compared with the maximum permissible torque. For a solid shaft with circular cross section, the maximum permissible torque, M_{max}, is given as follows:[31]

$$M_{max} = \frac{\tau \times J}{R} \quad [13]$$

where τ is the shear strength, J is the polar second moment of inertia, and R is the radius of the shaft. Considering the tool shoulder and tool pin as circular shafts, the polar second moment of inertia can be computed as follows:[31]

$$J = \int_A r^2 dA = \frac{\pi R^4}{2} \quad [14]$$

where r is the distance from the axis for a small area element dA. The tool pin is structurally the weakest part

of the tool as it has the minimum diameter. The maximum permissible torque for the cylindrically tapered tool pin with an average diameter of 5.33 mm, as used here, is about 16.1 Nm, considering the shear strength[32] of the tool material as 540 MPa at 613 K (340 °C). The shear strength values were not available at higher temperatures. Among the three optimum tool geometries, the maximum value of the computed torque on the pin is about 4.1 Nm. These values indicate that the tools with suggested optimum geometries can be used safely with a fairly high factor of safety. The tool design criterion considered here provides a reliable basis for the selection of an optimum tool shoulder diameter for a given rotational speed.

V. CONCLUSIONS

A three-dimensional, heat transfer and visco-plastic flow model was used to understand the effect of tool shoulder diameter on peak temperature, torque, and spindle power requirements in the FSW of AA7075-T6 at various rotational speeds. The increase in shoulder diameter resulted in higher peak temperature, spindle power, and torque requirements for all rotational speeds considered. As the shoulder diameter increases, the state of the deforming material changes from high flow stress and low temperature to low flow stress and high temperature. A design criterion for the selection of an optimum tool shoulder diameter is considered. The optimum tool shoulder diameter identified for 355, 560, and 710 rpm are 30, 25, and 20 mm, respectively. The mechanical energy provided by the tool is also shown to have a maximum for these combinations of optimal shoulder diameter and rotational speed. The computed peak temperature for these optimum tool shoulder diameters are found to lie well within the commonly used working range for FSW. The welds made at the optimum shoulder diameter and the corresponding tool rotation speed have shown acceptable YS and percent elongation (at break).

REFERENCES

1. H.K.D.H. Bhadeshia and T. DebRoy: *Sci. Technol. Weld. Join.*, 2009, vol. 14, pp. 193–96.
2. T. DebRoy and H.K.D.H. Bhadeshia: *Sci. Technol. Weld. Join.*, 2010, vol. 15, pp. 266–70.
3. R. Nandan, T.J. Lienert, and T. DebRoy: *Int. J. Mater. Res.*, 2008, vol. 99, pp. 434–44.
4. R. Nandan, G.G. Roy, T.J. Lienert, and T. DebRoy: *Acta Mater.*, 2007, vol. 55, pp. 883–95.
5. R. Nandan, G.G. Roy, T.J. Lienert, and T. DebRoy: *Sci. Technol. Weld. Join.*, 2006, vol. 11, pp. 526–37.
6. W.M. Thomas, E.D. Nicholas, J.C. Needham, M.G. Murch, P. Templesmith, and C.J. Dawes: ''Friction Stir Butt Welding'', International Patent Application No. PCT/GB92/02203 and GB Patent Application No. 9125978.8, Dec. 1991; U.S. Patent Application No. 5460317, Oct. 1995.
7. G. Buffa, J. Hua, and R. Shivpuri: *Mater. Sci. Eng. A*, 2006, vol. 419, pp. 381–88.
8. H. Fujii, L. Cui, and M. Maeda: *Mater. Sci. Eng. A*, 2006, vol. 419, pp. 25–31.
9. K. Kumar and S.V. Kailas: *Mater. Sci. Eng. A*, 2008, vol. 485, pp. 367–74.
10. Y.H. Zhao, S.B. Lin, L. Wu, and F.X. Qu: *Mater. Lett.*, 2005, vol. 59, pp. 2948–52.
11. Y.H. Zhao, S.B. Lin, F.X. Qu, and L. Wu: *Mater. Sci. Technol.*, 2006, vol. 22, pp. 45–50.
12. D.G. Hattingh, C. Bignaut, T.I Van Niekerk, and M.N. James: *J. Mater. Process. Technol*, 2008, vol. 203, pp. 46–57.
13. W.M. Thomas, K.I. Johnson, and C.S. Wiesner: *Adv. Eng. Mater.*, 2003, vol. 5, pp. 485–90.
14. W.M. Thomas: *Mater. Sci. Forum*, 2003, vols. 426–432, pp. 229–36.
15. P.A. Colegrove and H.R. Shercliff: *Sci. Technol. Weld. Join.*, 2004, vol. 9, pp. 345–51.
16. P.A. Colegrove and H.R. Shercliff: *Sci. Technol. Weld. Join.*, 2004, vol. 9, pp. 352–61.
17. R. Nandan, T. DebRoy, and H.K.D.H. Bhadeshia: *Prog. Mater. Sci.*, 2008, vol. 53, pp. 980–1023.
18. Z. Zhang, Y.L. Liu, and J.T. Chen: *Int. J. Adv. Manuf. Technol.*, 2009, vol. 45, pp. 889–95.
19. A. Scialpi, L.A.C. De Filippis, and P. Cavaliere: *Mater. Des*, 2007, vol. 28, pp. 1124–29.
20. R.M. Leal, C. Leitao, A. Loureiro, D.M. Rodrigues, and P. Vilaca: *Mater. Sci. Eng. A*, 2008, vol. 498, pp. 384–91.
21. K. Elangovan and V. Balasubramanian: *Mater. Des.*, 2008, vol. 29, pp. 362–73.
22. A. Arora, A. De, and T. DebRoy: *Scripta Mater.*, 2011, vol. 64, pp. 9–12.
23. R. Nandan, G.G. Roy, and T. DebRoy: *Metall. Mater. Trans. A*, 2006, vol. 37A, pp. 1247–59.
24. R. Nandan, B. Prabu, A. De, and T. DebRoy: *Weld. J.*, 2007, vol. 86, pp. 313s–322s.
25. A. Arora, R. Nandan, A. P. Reynolds, and T. DebRoy: *Scripta Mater.*, 2009, vol. 60, pp. 13–16.
26. A. Arora, Z. Zhang, A. De, and T. DebRoy: *Scripta Mater.*, 2009, vol. 61, pp. 863–66.
27. Q. Li and M. Lovell: *J. Mater. Process. Technol.*, 2005, vol. 160, pp. 245–56.
28. P.A. Colegrove and H.R. Shercliff: *Sci. Technol. Weld. Join.*, 2006, vol. 11, pp. 429–41.
29. P.A. Colegrove, H.R. Shercliff, and R. Zetter: *Sci. Technol. Weld. Join.*, 2007, vol. 12, pp. 284–97.
30. M.W. Mahoney, C.G. Rodes, J.G. Flintoff, R.A. Spurling, and W.H. Bingel: *Metall. Mater. Trans. A*, 1998, vol. 29A, pp. 1955–64.
31. E.J. Hearn: *Mechanics of Materials 1*, 3rd ed., Butterworth Heinemann, Oxford, United Kingdom, 1997, pp. 179–81.
32. J. Woolman and R.A. Mottram: *The Mechanical and Physical Properties of the British Standard En Steels (B.S. 970-1955)*, Pergamon, New York, NY, 1964, vol. 2, p. 107.